Organic & Biomolecular Chemistry

Accepted Manuscript

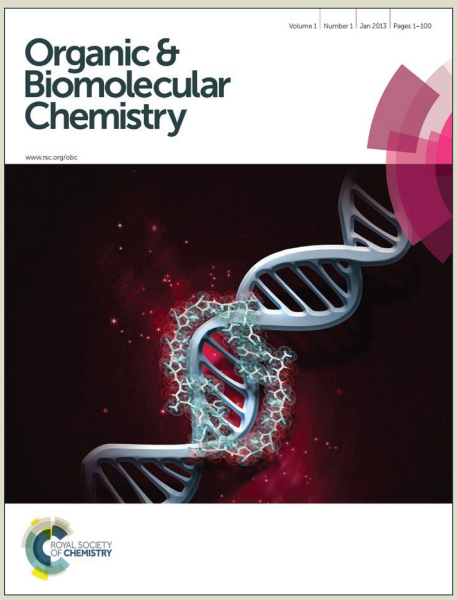

ROYAL SOCIETY OF CHEMISTRY

www.rsc.org/obc

Photocontrol of Ion Permeation in Lipid Vesicles with (Bola)amphiphilic Spirooxazines

Yamuna S. Kandasamy, Jianxin Cai, John G. Ottaviano, Kelti A. Smith, Ashley N. Williams, Jarod Moore, Kristen M. Louis, Lindsay Selzler, Alisha Beler, Tobechi Okwuonu and R. Scott Murphy*

Department of Chemistry and Biochemistry, Research and Innovation Centre, University of Regina, 3737 Wascana Parkway, Regina, SK, S4S 0A2, Canada

scott.murphy.uregina@gmail.com

Abstract

Three (bola)amphiphilic spirooxazines have been synthesized and their photochromism has been characterized. The large biphotochromic structure of **2** significantly affects its conformational flexibility and the rate constants for thermal ring closure are particularly dependent on the lipid phase state. Two comprehensive ion permeation studies were performed to examine the effect of spirooxazine inclusion and isomerization on membrane permeability. In all cases, the open-ring isomers of these spirooxazines are more disruptive in bilayer membranes than their closed-ring isomers. Further, the rate of ion permeation and net release are highly dependent on the lipid bilayer phase state and the relative position of the photochromic moiety in the bilayer membrane. Moreover, the difference in potassium ion permeability under UV and visible irradiation is more pronounced than previously reported photoresponsive membrane disruptors with reversible photocontrols.

Introduction

Biocompatible lipid vesicles that integrate photochromic molecules have shown potential in biomedical applications such as drug delivery and ion transport.[1-10] These photoresponsive systems provide a high level of spatial and temporal control for on-demand dosing. Further, photocontrols based on the reversible photoisomerization of photochromic molecules could be used to regulate the delivered dosage. To date, amphiphilic photochromic molecules comprised of azobenzene[11, 12], spiropyran[13], and dithienylethene[14] have been used to photocontrol ion permeation in lipid vesicles with varying degrees of success. For example, when an amphiphilic spiropyran was included into phosphatidylcholine (PC) vesicles the rate of potassium ion permeation increased.[13] Upon exposure to ultraviolet (UV) light the rate of ion permeation decreased, as the closed-ring spiro isomer was converted to the open-ring merocyanine isomer. However, the difference in permeability between these two isomeric states was within the experimental error and the observed perturbation order was not anticipated, as Hurst and coworkers admittedly desired a photochromic system that would promote ion leakage with UV irradiation.

Relatively few spirooxazine amphiphiles have been synthesized[15] and characterized in lipid vesicles.[16, 17] In addition, their photocontrol of ion permeability in lipid vesicles has never been examined, even though spirooxazines are well known for their greater resistance to photodegradation than the structurally related spiropyrans.[18, 19] Notably, spiropyrans specifically derived from the prevalent 6-nitro-BIPS core have been shown to have poor hydrolytic stability.[20-22] Surprisingly, the preparation of a bolaamphiphilic photochromic dimer has never been reported. Albeit, Fujiwara and coworkers have recently examined the photochromic reactivity of nonamphiphilic spirooxazine dimers in organic solution[23, 24], and their photocontrol of guest binding while tethered to a polymer.[25] Although the functionality achieved by these systems is slowly improving[26], biphotochromic systems have never been examined in lipid vesicles.

In an earlier report, we examined the thermal isomerization of **1** in lipid vesicles (Chart 1).[17] Consistent with similar spirooxazines,[16] the rate constant for thermal ring closure (k_T) increased and the wavelength of maximum absorption (λ_{max}) of the open-ring isomer underwent a small bathochromic shift with increasing solvent polarity. Upon inclusion of **1** in dipalmitoylphosphatidylcholine (DPPC) vesicles, the λ_{max} for the open-ring isomer underwent a hypsochromic shift relative to toluene, which suggested that the photochromic moiety of **1** is most likely located in the less polar aliphatic region of the bilayer membrane. Building on this previous work, we report on the synthesis of the first bolaamphiphilic biphotochromic dimer **2** and a new analogous amphiphilic spirooxazine **3**. Further, we have characterized their thermal isomerization in organic solution and lipid vesicles of varying lamellar phase, and have examined their reversible photocontrol of ion permeability (i.e., protons and potassium ions) through a bilayer membrane.

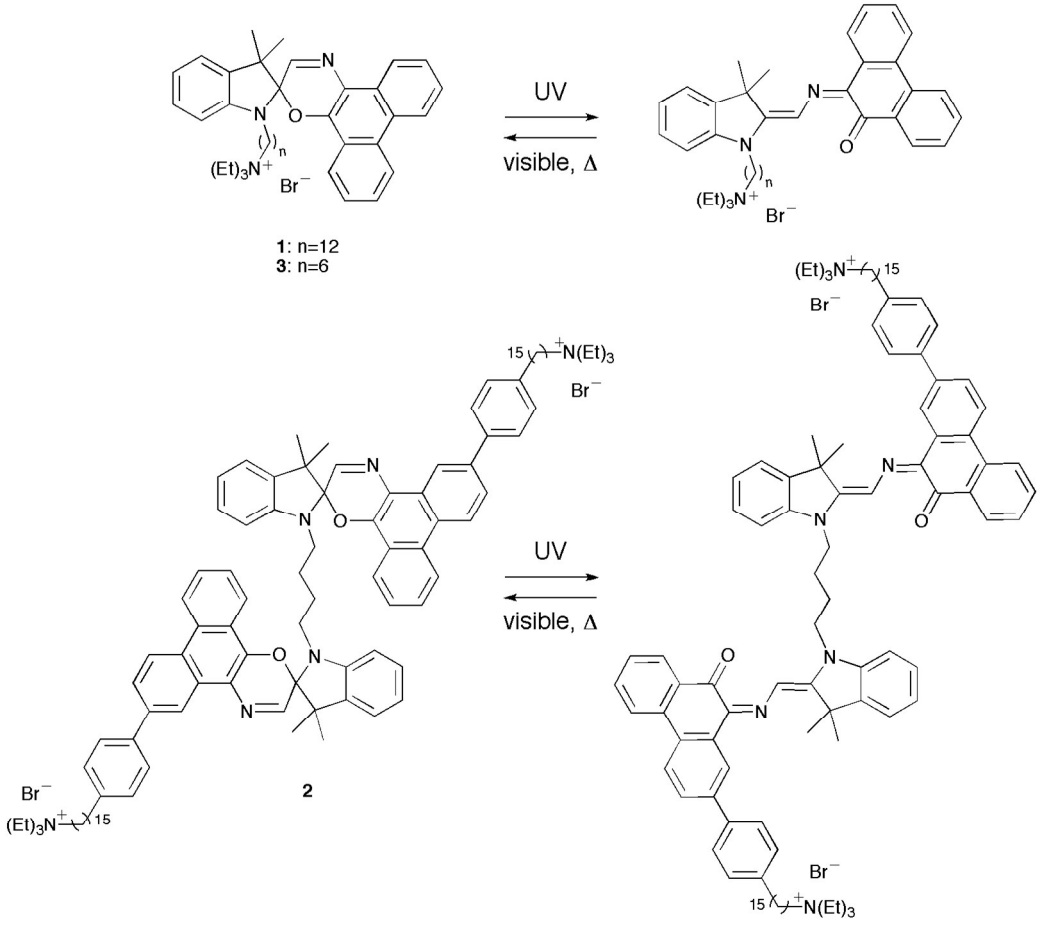

Chart 1. Structures of the (bola)amphiphilic spirooxazines photoisomers for **1**–**3**.

Results and discussion

Synthesis of 1–3. We have previously reported on the procedures for the synthesis of the amphiphilic spirooxazine **1**.[17] Similar procedures were used to prepare the analogous hexyl derivative, **3**. In general, the synthesis of the bolaamphiphilic spirooxazine dimer **2** involves the coupling of two moles of a substituted phenylboronic acid with a diiodospirooxazine dimer. We had originally prepared a substituted alkylboronic acid to couple with the diiodospirooxazine dimer; however, these attempts were unsuccessful due to the limited solubility of this alkylboronic acid. Also, lower reactivity is frequently observed in Suzuki-Miyaura reactions of alkylboronic acids when compared with arylboronic acids.[27] Consequently, our synthetic methodology began with the

inclusion of a cationic alkyl ammonium substituent on phenylboronic acid (Scheme 1). Initially, the Sonogashira reaction was used to couple 1-bromo-4-iodobenzene with pentadec-14-yn-1-ol to give **4** in moderate yield. The internal alkyne was then reduced by catalytic hydrogenation using hydrogen gas over platinum(IV) oxide to produce **5** in high yield. Notably, platinum(IV) oxide was used instead of the more common palladium on carbon because the former displays good chemoselectivity as debromination was not observed. *tert*-Butyldimethylsilyl chloride (TBSCl) and imidazole were then used to protect the terminal hydroxyl group of **5** to give **6** in good yield. The conversion of **6** to its corresponding boronic acid and subsequent protection using pinacol gave the boronate ester **7** in moderate yield. Deprotection of the hydroxyl group with hydrochloric acid in methanol produced **8** in high yield. Next, the primary alcohol was converted to the alkyl bromide using *N*-bromosuccinimide and triphenylphosphine to give **9** in moderate yield. The nucleophilic substitution of the alkyl bromide was achieved in high yield to produce the cationic quaternary ammonium substituent in **10** using triethylamine. This was followed by a convenient two-step procedure for the deprotection of the boronate ester.[28] The boronate ester was first converted to the potassium trifluoroborate salt **11** in good yield using potassium hydrogen fluoride. Treatment of the trifuoroborate salt with trimethylsilyl chloride afforded the corresponding boronic acid, which was used without further purification in the final coupling reaction with the diiodospirooxazine dimer **13**. This photochromic dimer was synthesized using phenanthrenequinone and 2,3,3-trimethylindolenine as starting materials for the preparation of the oxime **12** and the bisindoline unit, respectively. The iodination of phenanthrenequinone via an electrophilic aromatic substitution reaction produced 2-iodo-9,10-phenanthrenedione in low yield due to the formation of a side product, 2,6-diiodophenanthrenequinone, and the presence of unreacted starting material. The conversion of the diketone to the oxime **12** was considerably more successful. The precursor to the bisindoline unit was a bisindoleninium bromide salt. This salt was prepared from successive

nucleophilic substitution reactions of 1,4-dibromobutane with excess 2,3,3-trimethylindolenine. Subsequently, the bisindoleninium bromide salt was converted to the bisindoline unit with base in moderate yield. Thereafter, **13** was formed from the electrocyclic reaction of the bisindoline unit and **12**. The Suzuki-Miyaura reaction was then used to couple two moles of the substituted phenylboronic acid with **13** to produce the final bolaamphiphilic spirooxazine dimer **2**.

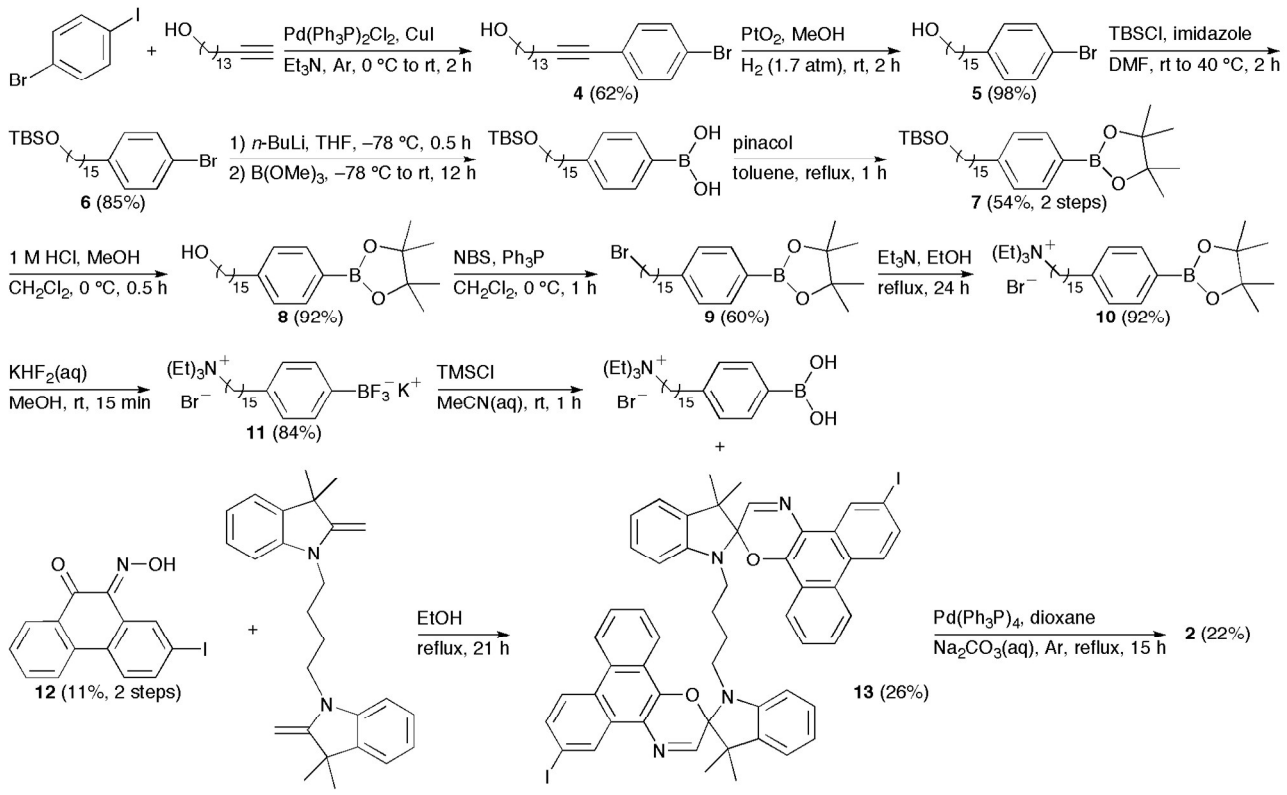

Scheme 1. Synthesis of **2**.

Photochromism of 1–3. Absorption in the visible region was observed for all spirooxazines prior to irradiation with UV light. The thermochromic behavior of analogous phenanthryl-based spirooxazines has been well established in homogeneous solution[29-32], micelles[33], and lipid vesicles[16, 17]. Further, this thermal equilibrium has been shown to favour the formation of the open-ring isomer as the polarity of the microenvironment increases.[33] Upon UV irradiation, spirooxazine

absorption increased further in the visible region, which represents the formation of the open-ring isomer. In addition, the photoisomerization of **1**–**3** was reversible in organic solution and lipid vesicles. Unfortunately, we were unable to differentiate between the open-ring–closed-ring and the open-ring–open-ring isomers of **2** as the two photochromic units are not electronically conjugated. Nonetheless, following UV irradiation, thermal equilibration led to a decrease in absorbance at the λ_{max} in the visible region giving back the absorbance spectrum prior to UV irradiation. The rate constants for thermal ring closure (k_T) were determined from exponential fits of the absorbance decays at λ_{max}. We measured the k_T for **1**–**3** in acetonitrile and toluene to examine the effect of solvent polarity and molecular structure on the thermal ring closure (Table 1). The k_T for **1** and **3** were both five fold larger in acetonitrile than toluene. Although **2** was not soluble in toluene, the precursor **13** was examined in both solvents. Similarly, k_T for **13** was 18 fold larger in acetonitrile than toluene. Consistent with reports on analogous phenanthryl-based spirooxazines[16, 17, 29, 30, 34], these results suggest that k_T for **1**–**3** increase with increasing solvent polarity. Furthermore, k_T for **1** and **3** in acetonitrile and toluene were within experimental error of each other. Therefore, the difference in the alkyl chain length has a minor effect on thermal ring closure in organic solution. However, these rate constants in acetonitrile were two fold larger than **2**. A similar reduction in k_T has been reported for a biphotochromic system when compared with its corresponding monomer.[34] This suggests that the dimeric structure of **2**, specifically the linked indoline moieties, does influence the rate of ring closure through a steric effect.

The k_T for **1**–**3** were also measured in two different lipid systems, namely DPPC and 1,2-dioleoyl-*sn*-glycero-3-phosphocholine (DOPC), to examine the effect of the lipid bilayer phase state on the rate of thermal ring closure. In addition, the activation energies for ring closure of **1**–**3** in lipid vesicles were determined from their Arrhenius behavior. The phase state of these lipid systems is dependent on temperature. At ambient temperature, DPPC vesicles are in the gel phase,

whereas DOPC vesicles are in the fluid phase.[35] The k_T for **1** and **3** were two fold larger in DOPC vesicles than DPPC vesicles. This trend was anticipated given that local viscosity of DPPC bilayers in their gel phase is higher and more restrictive to isomerization than DOPC bilayers in their fluid phase. In addition, k_T is at least 50% larger for **1** when compared with **3** in both lipid systems.

Table 1 Thermal ring closure rate constants (k_T) for spirooxazines in organic solution and lipid vesicles at a mole ratio of 1:20 (i.e., spirooxazine/lipid)[a]

	k_T (10^{-1} s^{-1})			
SpOx	Acetonitrile	Toluene	DPPC	DOPC
1	4.16 ± 0.12 (590)	0.78 ± 0.02 (591)	0.83 ± 0.01 (589)	1.91 ± 0.06 (584)
2	2.14 ± 0.12 (600)	N/A	0.079 ± 0.002[b] (610)	0.48 ± 0.03[b] (606)
			0.011 ± 0.002[b]	0.10 ± 0.01[b]
3	4.45 ± 0.48 (595)	0.81 ± 0.18 (598)	0.56 ± 0.07 (608)	1.03 ± 0.02 (606)
13	3.14 ± 0.16 (600)	0.17 ± 0.01 (597)	N/A	N/A

[a] The error is the standard deviation for the mean taken from a minimum of three independent measurements, which were recorded at, or extrapolated to 7 °C. The absorption maximum of the open-ring isomer is shown in parentheses and the error is ± 1 nm. [b] The rate constants were obtained from biexponential fits.

This latter result suggests that the relative positioning of the photochromic moiety of **1** and **3** in the lipid bilayer is different owing to differences in alkyl chain length. A similar trend has been previously observed for spiropyrans with assorted alkyl chain lengths in lipid vesicles.[36] Specifically, Wohl and coworkers examined the free volume distribution in a DPPC lipid bilayer. In this work, the largest available free volume was detected near the bilayer midplane, while the smallest free volume was found in the highly ordered region of the hydrocarbon chains. Since the polarity in these regions of the bilayer is similar[37], the viscosity of the microenvironment will have a dominant effect on k_T. Consequently, we postulate that the thermal ring closure of **1** is less

hindered as it is most likely positioned closer to the less dense bilayer midplane, thereby enhancing rates. Not surprisingly, k_T for **2** was significantly smaller when compared with the monomer systems. Interestingly, kinetic decays with biexponential behavior were observed for **2** in DPPC and DOPC vesicles (Figure 1). Time-resolved studies on phenanthryl-based spirooxazines have previously attributed this biexponential character to the *cis-trans* isomerization of the open-ring isomer prior to ring closure.[17, 30] Our ability to observe this shorter-lived component in lipid vesicles highlights the reduced conformational flexibility of the dimer system due to the higher viscosity within the bilayer membrane when compared with organic solution. Analogous to the monomer systems, the longer-lived component of the thermal decay for **2** was nine fold larger in DOPC vesicles than DPPC vesicles. Compared with the monomer systems, k_T for **2** was 75 and 50 fold smaller than **1** and **3** in DPPC vesicles, and 20 and 10 fold smaller in DOPC vesicles, respectively. Also, the activation energies for the thermal ring closure of **1**, **2**, and **3** were 97, 119 and 104 kJ mol^{-1} in DPPC vesicles, and 87, 74 and 84 kJ mol^{-1} in DOPC vesicles, respectively, over a temperature range of 2–21 °C (Figures S1–S6, ESI). Thus, the activation energies are higher in the more viscous gel phase of DPPC vesicles than the fluid phase of DOPC vesicles. This correlation with lipid phase state is consistent with a similar examination of spiropyrans in DPPC vesicles.[36] Again, these results demonstrate the increased rigidity of a DPPC bilayer when compared with a DOPC bilayer, and the effect of a more viscous microenvironment on the thermal ring closure of these (bola)amphiphilic spirooxazines. Overall, the isomerization kinetics show that the larger molecular structure of **2** greatly affects the conformational mobility necessary for ring closure when compared with the monomer systems.

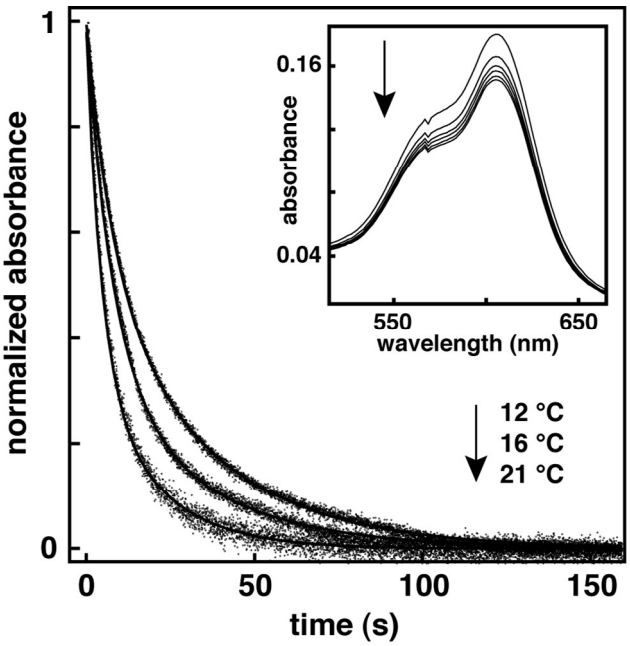

Figure 1. Normalized decay kinetics for the open-ring isomer of **2** in DOPC vesicles at a mole ratio of 1:20 (i.e., spirooxazine/lipid) monitored at 606 nm following irradiation with UV light, and recorded at various temperatures. The inset is a series of absorption spectra recorded in the visible region at 12 °C following a 20 s irradiation with UV light, as the open-ring isomer reverts back to the closed-ring isomer.

Proton permeation studies in lipid vesicles. A fluorescence assay[14, 38, 39] was used to assess the photocontrol of proton permeability for lipid vesicles incorporating spirooxazines **1**–**3**. In this assay, the photoresponsive lipid vesicles entrap a pH-sensitive, fluorescent probe, 8-hydroxypyrene-1,3,6-trisulfonic acid (HPTS). Then a transmembrane pH gradient is formed by adding base to the external buffer. The collapse of this pH gradient is monitored over time from changes in the fluorescence of HPTS. Subsequently, the fluorescence data is converted to a normalized extent of permeation (N) from which the rate constant for proton permeation (k_{H+}) is determined (Figure S7, ESI). In general, the pH gradient is expected to collapse more rapidly if the incorporation of spirooxazines as either photoisomer enhances membrane permeability. The permeation of protons across bilayer membranes has been described by a sequential two-step mechanism.[40] This biphasic

route proceeds from a transient–pore phase to a solubility–diffusion phase. During the transient–pore phase, which is initiated by the addition of base, a steep rise in *N* is often observed. This increase in proton permeation is due to the formation of transient hydrated pores within the bilayer produced by thermal fluctuations as the vesicles adjust to both the electrical potential and osmotic gradients formed by the rapid change in pH.[41] Once both gradients are closer to equilibrium a relatively slower rate of proton permeation is observed. This second phase of proton permeation is consistent with the solubility–diffusion model whereby hydrated protons partition into the inner leaflet of the bilayer, diffuse through the hydrophobic core, and partition out of the outer leaflet into the external buffer.[40] The rate constants presented in this study were determined from this second phase of proton permeation because permeation during this phase best represents the effect of spirooxazine inclusion and isomerization on membrane permeability.

We have recently reported on the photocontrol of proton permeation in lipid vesicles including thermally irreversible, amphiphilic dithienylethene monomers using the same fluorescence assay described here.[14] In that report, we examined pure lipid vesicles to provide a comparison with vesicles incorporating dithienylethenes. This was necessary given the moderate batch-to-batch variability normally observed in lipid vesicle studies.[14, 38] Correspondingly, we re-examined the k_{H+} and *N* for DOPC and DPPC control vesicles. Consistent with our earlier study[14], the rate constants and *N* were four fold higher in DOPC than DPPC (Table 2), confirming that DOPC vesicles are more permeable to protons than DPPC vesicles. In addition, the changes in k_{H+} and *N* following UV irradiation were also similar. Overall, the proton leakage observed in pure lipid vesicles occurs primarily during the transient–pore phase following the formation of the transmembrane pH gradient. Nonetheless, comparisons with these control samples will ensure that changes in membrane permeability are related to the inclusion and isomerization of **1**–**3** in lipid vesicles.

The k_{H+} and N were initially examined for amphiphilic spirooxazines **1** and **3** in DOPC and DPPC vesicles to assess the effect of the position of the photochromic moiety on membrane permeability. Varying the alkyl chain length has been shown to be an effective approach for controlling the embedding depth of the photochromic moiety in bilayer membranes.[36] Prior to UV irradiation, k_{H+} for **1** in DOPC vesicles at a mole ratio of 1:30 **1**/DOPC was two fold higher than the control vesicles, whereas, k_{H+} for **3** in DOPC vesicles was similar to the control vesicles (Table 2). However, N for **1** and **3** were both two fold higher than the control vesicles prior to the addition of detergent, which might suggest that **1** and **3** are equally disruptive overall in DOPC vesicles. Yet, N immediately following the addition of base is lower for **1** when compared with **3** (Figure 2). These results suggest that the presence of **3** with a shorter hexyl chain enhances proton permeation during the transient–pore phase but provides no significant increase during the solubility–diffusion phase when compared with **1**. Conversely, the inclusion of the **1** with a longer dodecyl chain appears to provide moderate stability during the transient–pore phase yet the rate of proton permeation is two fold higher than **3** during the solubility–diffusion phase. Overall, the inclusion of amphiphilic spirooxazine monomers does disrupt bilayer packing in DOPC vesicles. Although, the extent of the disruption is dependent on a combination of factors: the relative position of the photochromic moiety in the bilayer membrane and the phase during which proton permeation occurs.

Table 2 Proton permeation rate constants and normalized extent of proton permeation determined for **1**–**3** in DOPC and DPPC vesicles at a mole ratio of 1:30 spirooxazine/lipid[a]

DOPC	k_{H+} (10^{-4} s^{-1})		*N*	
UV	No	Yes	No	Yes
Control	1.8 ± 0.5 (57)	1.4 ± 0.6 (52)	0.31 ± 0.07 (47)	0.37 ± 0.06 (45)
1	4.3 ± 0.4 (6)	4.1± 0.2 (6)	0.57 ± 0.02 (6)	0.62 ± 0.05 (6)
2	8.9 ± 0.6 (6)	8.7 ± 0.2 (6)	0.89 ± 0.01 (7)	0.90 ± 0.01 (6)
3	1.8 ± 0.1 (6)	1.7 ± 0.4 (6)	0.57 ± 0.03 (6)	0.61 ± 0.03 (6)
DPPC	k_{H+} (10^{-4} s^{-1})		*N*	
UV	No	Yes	No	Yes
Control	0.42 ± 0.24 (61)	0.31 ± 0.27 (52)	0.07 ± 0.05 (54)	0.20 ± 0.07 (49)
1	1.1 ± 0.3 (6)	0.99 ± 0.50 (6)	0.65 ± 0.05 (6)	0.71 ± 0.07 (6)
2	1.0 ± 0.3 (6)	0.83 ± 0.35 (6)	0.53 ± 0.11 (6)	0.62 ± 0.09 (6)
3	1.7 ± 0.6 (6)	1.4 ± 0.6 (6)	0.22 ± 0.06 (6)	0.40 ± 0.09 (6)

[a] The error is the standard deviation of the mean taken from *n* independent measurements. The value of *n* is shown in parentheses.

Following UV irradiation no significant change in k_{H+} or *N* was observed for **1** or **3** when compared to the nonirradiated vesicles. This was somewhat anticipated given that thermal reversion to the closed-ring isomers at room temperature is most likely complete prior to the formation of the transmembrane gradient. Consequently, this fluorescence assay is not ideal for assessing the photocontrol of membrane permeability for thermally reversible photochromic molecules in lipid vesicles. Nevertheless, this assay does provide a sensitive method for evaluating the relative effect of spirooxazine inclusion on the membrane permeability of lipid vesicles. As a result, we have also examined these systems using a potassium ion permeation assay to better assess the effect of spirooxazine isomerization on membrane permeability (vide infra).

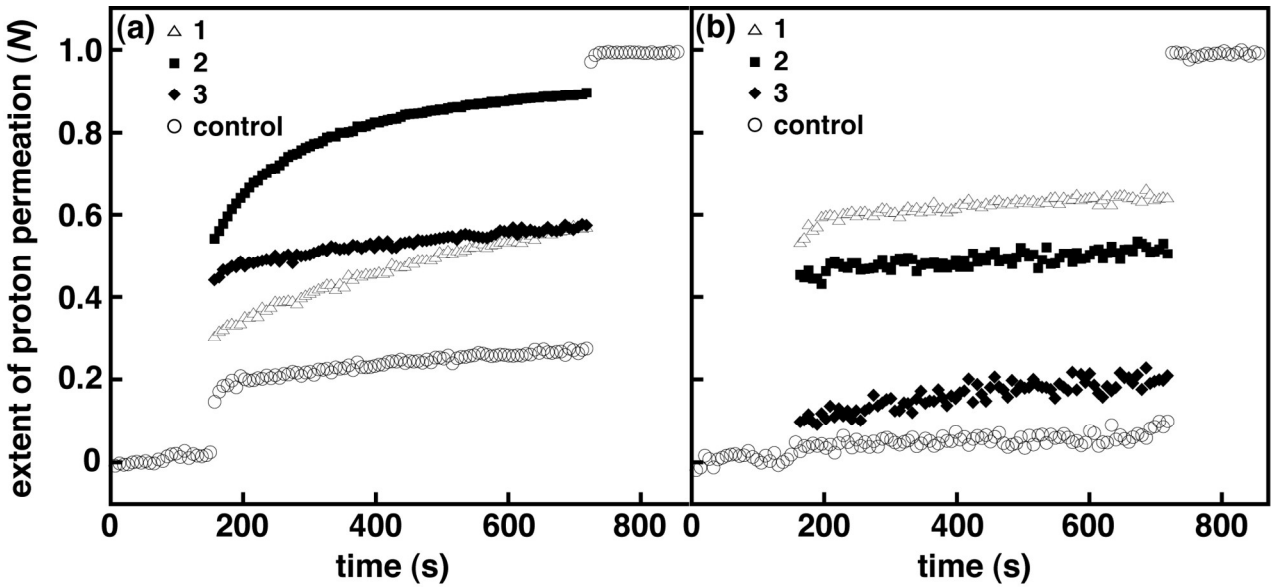

Figure 2. Normalized extent of proton permeation as a function of time for **1**–**3** in DOPC (a) and DPPC (b) vesicles at a mole ratio of 1:30 (i.e., spirooxazine/lipid) prior to UV irradiation. For clarity error bars are not shown, and only the control is shown before the base pulse and after the addition of detergent.

In DPPC vesicles, k_{H+} for **1** and **3** at a mole ratio of 1:30 were at least three fold higher than the control vesicles (Table 2). In addition, *N* for **1** and **3** were nine and three fold higher when compared with the control vesicles, respectively (Figure 2). Given the k_{H+} for **1** and **3** are within experimental error of one another, the large difference in *N* suggests that the inclusion of a spirooxazine with a longer alkyl chain significantly enhances proton permeation during the transient–pore phase for lipid vesicles in the rigid gel phase. Thus, **1** is more disruptive in DPPC vesicles because the photochromic moiety is presumably more deeply embedded in the bilayer membrane. Also, the relative change in k_{H+} and *N* for both monomers is greater in DPPC vesicles than those observed in DOPC vesicles when compared to their respective control vesicles. A similar trend with the phase state of the lipid vesicles has also been observed for amphiphilic dithienylethenes.[14] Like **1** and **3** in DOPC vesicles, there was no significant change in k_{H+} in DPPC vesicles following UV irradiation. However, there was a two fold increase in *N* for **3** but no significant change was observed for **1**. This suggests that the photoisomerization of the hexyl chain analogue disrupts the bilayer

membrane to a greater extent than the dodecyl analogue in DPPC. Yet, one must be cautious considering *N* for the DPPC control vesicles also increases with irradiation. Interestingly, at lower concentrations of **3** in DPPC vesicles (i.e., 1:40 **3**/DPPC; Table S1 and Figure S2, ESI) a four fold increase in *N* was observed following irradiation, whereas at higher concentrations (i.e., 1:20) no significant change was seen. Given this concentration dependence on *N*, we suggest that these changes are more of a reflection of the higher stability of nonirradiated DPPC vesicles, and those incorporating low concentrations of spirooxazines, than solely due to the photoisomerization of **3**. That is, the inclusion of spirooxazines at higher concentrations is the primary contributor to a decrease in vesicle stability and an increase in *N*. To support this proposal further, we determined *N* for both **1** and the dimer **2** in DPPC at 1:50 (Tables S2 and S3, and Figures S9 and S11, respectively, ESI) and found that both were two fold higher following irradiation. Yet at 1:30, both spirooxazines had similar *N*. Overall, the inclusion of the dodecyl derivative in DPPC vesicles appears to be more disruptive than the hexyl derivative in both nonirradiated lipid systems at 1:30 because k_{H+} is two fold larger in DOPC and *N* is three fold larger in DPPC. As a result, these studies provide additional support to the hypothesis that the relative position of the photochromic moiety in the bilayer membrane is important to vesicle permeability. Interestingly, the effect of chain length on membrane permeability is more pronounced for these spirooxazines than the series of dithienylethenes we recently examined.[14] This particular comparison suggests that vesicle stability is more sensitive to the relative location of a spirooxazine than a dithienylethene, and the former may be a more effective membrane disruptor.

The bolaamphiphilic spirooxazine **2** was also examined using the fluorescence assay to determine if the inclusion of a larger dimer is a more disruptive to a bilayer membrane than a monomer like **1**. Ideally, we envisage **2** spanning a bilayer membrane by positioning charged tethers within the hydrophilic headgroup region of the inner and outer leaflets. However, it is

possible that the dimer may adopt a U-shaped or folded conformation in lipid vesicles where both charged tethers reside in a single leaflet. Nonetheless, the inclusion of **2** should cause greater disruption than a monomer that resides in only one leaflet. The k_{H+} for **2** in DOPC vesicles at a mole ratio of 1:30 was five fold higher than the control vesicles, and three and five fold higher than **1** and **3** in DOPC vesicles, respectively (Table 2). Also, N for **2** in DOPC vesicles was three fold higher than the control vesicles, and 50% higher than both **1** and **3** in DOPC vesicles. We postulate that the higher k_{H+} and N values are correlated with the increased molecular size of **2** when compared with the monomer systems. In DPPC vesicles, **2** also exhibited a large increase in proton permeation but it was similar to that observed for the monomeric spirooxazines. Following UV irradiation, and similar to **1** and **3**, changes in k_{H+} and N for **2** in both DOPC and DPPC vesicles were within experimental error of the nonirradiated samples. Thus, photoisomerization and the subsequent thermal isomerization back to the closed-ring isomer of **2** prior to the addition of base does not have a significant effect on the permeability or the overall integrity of these lipid vesicles. Notably, k_{H+} is nine fold higher in DOPC vesicles than in DPPC vesicles, which demonstrates the importance of the lipid bilayer phase state on membrane permeability. In fact, the curvature observed for the plot of **2** in DOPC vesicles following the addition of base is more pronounced than the other systems, which qualitatively indicates that the rate of proton permeation is fast (Figure 2). Interestingly, the molecular size of these spirooxazines is positively correlated with k_{H+} in DOPC vesicles. This suggests that a structure–activity relationship does exist within this series of photochromic molecules. By contrast, this relationship is not observed in DPPC vesicles, as k_{H+} was similar for all three molecules. As a result, this lack of selectivity implies that the inclusion of spirooxazines in gel phase lipid vesicles exhibits an 'all-or-nothing' activity, whereas in fluid phase lipid vesicles spirooxazine structure is important to activity. Like the spirooxazine comparisons presented here, k_{H+} for **2** was at least three fold higher than the dithienylethene monomers in DOPC

vesicles, which further supports our hypothesis that molecular size is correlated with membrane permeability in fluid phase vesicles. In addition, similar to our observations with spirooxazines, there was no correlation between k_{H+} and the molecular size of the dithienylethenes in DPPC vesicles.

To measure the effect of spirooxazine concentration on vesicle permeability, we examined **1**–**3** in lipid vesicles at various mole ratios. As expected, the spirooxazine concentration in DOPC and DPPC vesicles do affect both k_{H+} and N. However, the magnitude of these changes was dependent on the spirooxazine–lipid system studied. Increasing the mole ratio of **2** from 1:30 to 1:20 in both DOPC and DPPC resulted in unstable lipid vesicles and complete collapse of the pH gradient as shown from N values approaching unity (Table S3, and Figures S10 and S11, ESI). Decreasing the mole ratio to 1:50 significantly reduced proton leakage three fold in DPPC vesicles, but had a relatively small effect in DOPC vesicles. However, both lipid vesicles were two fold more permeable than their respective controls. In DOPC vesicles, the k_{H+} increased 50% from 1:50 to 1:30, whereas in DPPC vesicles the k_{H+} was constant over the same concentration range. Again, this highlights the effect of the lipid bilayer phase state on the observed behavior. In DPPC vesicles, N is dependent on concentration, whereas k_{H+} is not. Conversely, in DOPC vesicles k_{H+} is dependent on concentration, but N is moderately dependent. These trends suggest that the lipid bilayer phase state affects the predominant mechanism that governs permeation through the bilayer membrane. That is, the inclusion of **2** primarily affects proton permeation during the solubility–diffusion phase in fluid phase vesicles, whereas in gel phase vesicles permeation is largely altered during the transient–pore phase. Similar to **2**, the k_{H+} were reasonably correlated to the concentration of **3** in DOPC vesicles, although the changes were small by comparison. Unlike **2**, DPPC and DOPC vesicle stability was compromised only when **3** was incorporated at a higher mole ratio of 1:10 (Table S1, and Figures S8 and S12, ESI). This suggests that the inclusion of the

amphiphilic monomer is relatively less disruptive in lipid vesicles than the larger bolaamphiphilic dimer. Interestingly, the highest mole ratio at which lipid vesicles incorporating **1** were not compromised was dependent on the lipid bilayer phase state. In DPPC, vesicle stability was compromised when **1** was included at a mole ratio of 1:20 but stable in DOPC vesicles at a mole ratio of 1:10, although they were very permeable (Table S2, and Figures S9 and 3, ESI). All together, the permeability of DOPC vesicles incorporating these (bola)amphiphilic spirooxazines is found to increase in the order of **3** ≤ **1** < **2** when one considers both k_{H+} and N collectively. Yet for DPPC vesicles, permeability increases in the order of **3** < **1** ≈ **2**. Once again, these differences in relative permeability indicate that the lipid bilayer phase state and spirooxazine structure are important to vesicle integrity prior to UV irradiation.

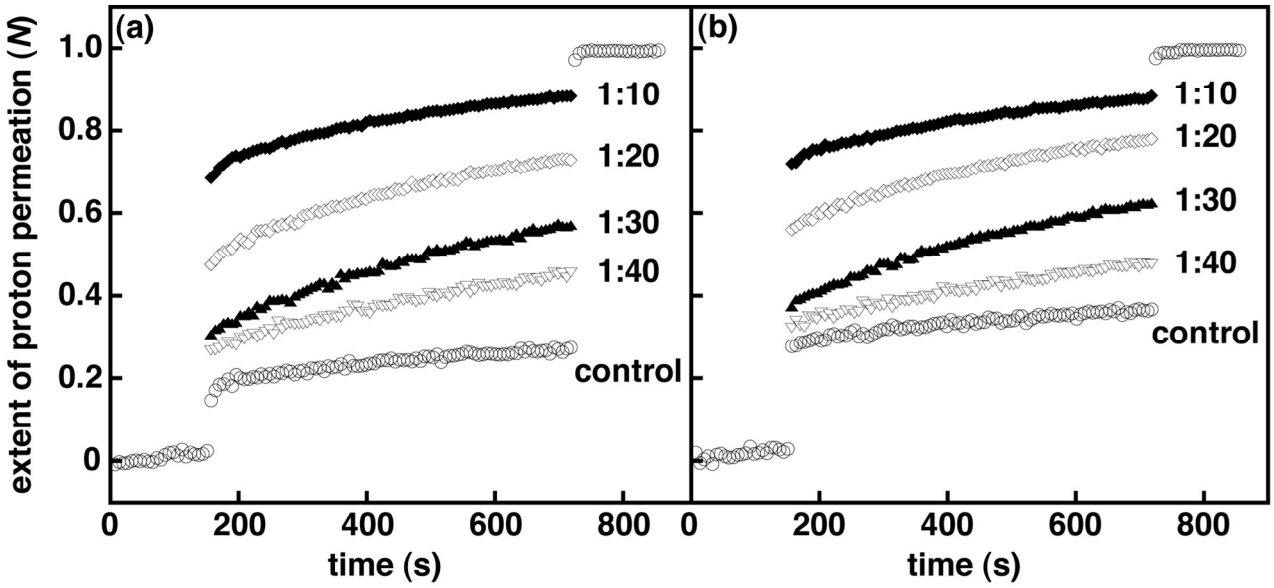

Figure 3. Normalized extent of proton permeation as a function of time for various mole ratios of **1** in DOPC vesicles (i.e., **1** /DOPC) prior to UV irradiation (a) and after 3 min of UV irradiation (b). Each plot is an average of a minimum of six independent measurements. For clarity error bars are not shown, and only the control is shown before the base pulse and after the addition of detergent.

Potassium ion permeation studies in lipid vesicles. As discussed earlier, the fluorescence assay is not ideal for evaluating the reversible photocontrol of membrane permeability for thermally reversible photochromic molecules in lipid vesicles. In practice, the fluorescence assay is sensitive to background, scattered light such that the measurement must be stopped while the irradiation source is illuminated. In order to monitor changes in permeability uninterrupted with continuous irradiation, an assay that is not sensitive to background light is required. As a result, we have also examined spirooxazines in lipid vesicles using a potassium ion permeation assay to better assess the effect of spirooxazine isomerization on membrane permeability. This assay was used to determine the rate constant for potassium ion permeation (k_{K+}) and the percentage of potassium ion release (% release). Initially, the k_{K+} and % release were determined for DOPC and DPPC control vesicles prior to, and following irradiation with UV and visible light. Consistent with fluorescence assay, DOPC vesicles are more permeable to potassium ions than DPPC vesicles. In all cases, both the k_{K+} and % release were at least two fold higher in DOPC than DPPC vesicles (Table 3, and Figures 4 and S13, ESI). Following UV irradiation a 50% increase in k_{K+} and % release was also observed for DOPC vesicles, whereas for DPPC vesicles the changes were within experimental error of the nonirradiated samples. The changes observed for DOPC vesicles may stem from the susceptibility of the unsaturated double bonds in the DOPC lipid tails to photooxidation, which can increase membrane permeability.[42-45] By contrast, visible irradiation had no significant effect on k_{K+} for either lipid system. In general, the efflux detected from the control samples is largely due to the high concentration gradient and occurs primarily via the solubility-diffusion mechanism. Still, comparisons with these control samples will ensure that changes in membrane permeability are related to the inclusion and isomerization of **1**–**3** in lipid vesicles.

Prior to irradiation, the k_{K+} for both **1** and **3** in DPPC vesicles at a mole ratio of 1:20 were three fold higher than the control vesicles, whereas in DOPC vesicles, they were 50% higher. This

Table 3 Potassium ion permeation rate constants and normalized percentage of potassium ion release determined for **1**–**3** in DOPC and DPPC vesicles at a mole ratio of 1:20 spirooxazine/lipid[a]

DOPC	k_{K+} (10^{-8} M s^{-1})			% release	
Light	No	UV	Visible	No	UV and Visible[b]
Control	1.4 ± 0.1	2.1 ± 0.1	1.9 ± 0.1	15 ± 1	21 ± 2
1	2.1 ± 0.1	4.7 ± 1.1	0.3 ± 0.2	29 ± 4	49 ± 1
2	2.7 ± 0.1	3.9 ± 0.5	1.4 ± 0.3	33 ± 1	54 ± 3
3	2.0 ± 0.1	4.0 ± 0.2	0.9 ± 0.2	25 ± 3	41 ± 2
DPPC	k_{K+} (10^{-8} M s^{-1})			% release	
Light	No	UV	Visible	No	UV and Visible[b]
Control	0.7 ± 0.1	0.8 ± 0.1	0.6 ± 0.1	6 ± 1	7 ± 1
1	1.8 ± 0.1	2.8 ± 0.4	2.7 ± 0.4	21 ± 1	39 ± 3
2	1.6 ± 0.1	4.0 ± 0.5	2.8 ± 0.2	18 ± 3	60 ± 5
3	1.9 ± 0.1	2.6 ± 0.3	2.4 ± 0.2	24 ± 1	34 ± 1

[a] The error is the standard deviation of the mean taken from three independent measurements.
[b] The percentage of potassium ion release was determined after 3.5 cycles of UV and visible light irradiation.

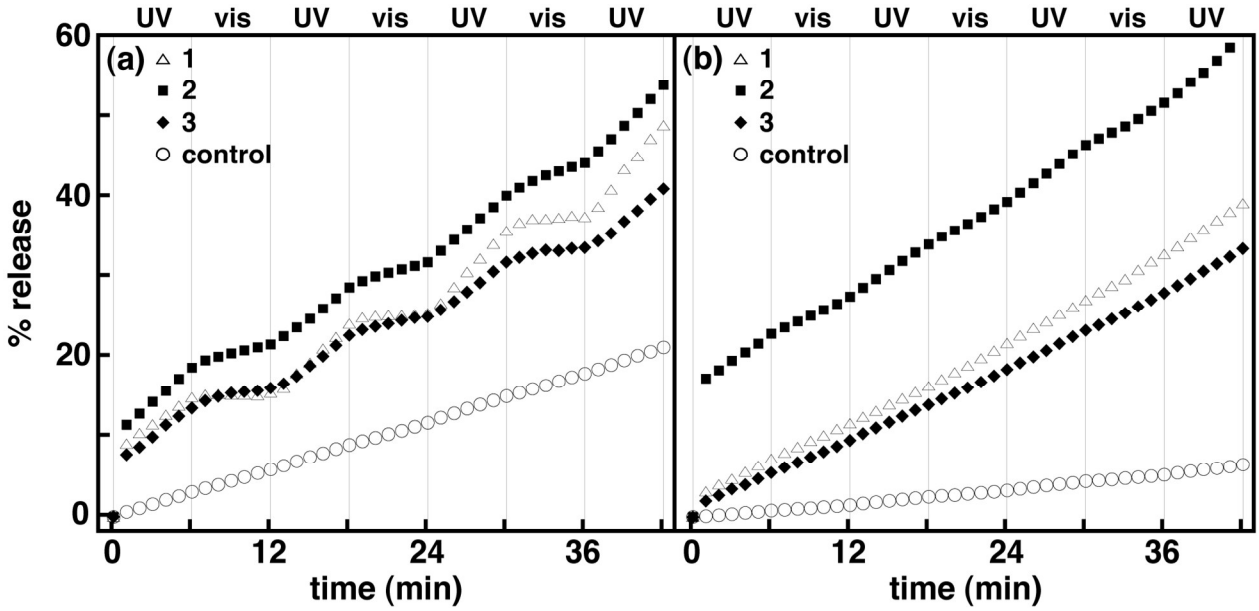

Figure 4. Normalized percentage of potassium ion release as a function of time for **1**–**3** in DOPC (a) and DPPC (b) vesicles at a mole ratio of 1:20 (i.e., spirooxazine/lipid) with alternating periods of continuous UV and visible irradiation. Each plot is an average of three independent measurements. For clarity error bars are not shown.

similarity in k_{K+} for **1** and **3** suggests that the alkyl chain length has little effect on the permeation of potassium ions in both lipid systems. The % release for **1** and **3** were also similar at two and four fold higher in DOPC and DPPC vesicles than the control vesicles, respectively. The results of this assay are consistent with the fluorescence assay in that the inclusion of amphiphilic spirooxazine monomers does disrupt bilayer packing in DOPC and DPPC vesicles and increases their permeability. However, the two fold difference observed in k_{H+} between **1** and **3** in DOPC vesicles was not evident in this assay. This variance highlights the increased sensitivity of the fluorescence assay to changes in molecular structure given proton permeation can also occur by the Grotthuss mechanism (i.e., hopping along hydrogen-bonded chains of water), which is not available to potassium ions.[41] Upon UV irradiation, k_{K+} for both **1** and **3** in DOPC vesicles increased two fold. In DPPC vesicles, a small increase was also observed. These results suggest that photoisomerization of spirooxazines to their more polar ring-opened form leads to greater

disruption of the local bilayer structure, which allows for increased water penetration and enhanced permeability. Interestingly, the k_{K+} for both **1** and **3** in DOPC vesicles were significantly lower upon irradiation with visible light to below control levels. Specifically, **1** and **3** were fourteen and four~~teen~~ fold lower than those observed following UV irradiation, respectively. The large changes observed in these rate constants suggest that isomerization to the less polar closed-ring isomers restores the normal bilayer membrane structure, significantly reducing permeation rates. In addition, the rate constants were lower than the nonirradiated samples, which suggest that an equilibrium mixture of both isomers exists in DOPC vesicles prior to irradiation. This thermal equilibrium is a consequence of the thermochromic behavior of these spirooxazines. By comparison, the k_{K+} for both **1** and **3** in DPPC vesicles were relatively unchanged upon irradiation with visible light. The % release for these systems was also measured after several cycles of alternating UV and visible irradiation. In DPPC vesicles, the net change in % release for **1** and **3** was nineteen and nine fold higher than the control vesicles, respectively. In DOPC vesicles, both spirooxazines were two fold higher than the controls. Similar to the fluorescence assay, we also accredit the relative magnitude of these changes to the higher stability of gel phase DPPC vesicles, which are three fold less permeable than the fluid phase DOPC vesicles. Once again, the dodecyl derivative appears to be a more disruptive than the hexyl derivative in both lipid systems because k_{K+} upon UV and visible irradiation underwent the largest change in DOPC vesicles and the net change in % release was largest in DPPC vesicles. These studies are consistent with the fluorescence assay analysis and further support our hypothesis that the relative position of the photochromic moiety in the bilayer membrane is important to vesicle permeability. Intriguingly, the photocontrol of potassium ion permeation from lipid vesicles incorporating a spiropyran with a single alkyl chain has been reported previously.[13] Unlike **1** and **3**, this spiropyran did not contain a terminally charged ammonium group. As a result, the perturbation order for controlling membrane

permeability was reversed when compared with our systems. That is, the closed-ring isomers caused greater disruption of the local bilayer structure than the open-ring isomers. This opposing result suggests that the inclusion of a terminally charged 'tether' improves the organization of the spirooxazines within the bilayer membrane, enhancing membrane stability. Consequently, this comparison clearly shows that the perturbation order can be conveniently controlled through the insertion or deletion of this structural feature. In addition, the differences in potassium ion permeability under UV and visible irradiation are considerably more pronounced for these spirooxazines than the spiropyran derivative previously reported.

Similarly, **2** was examined to determine if the isomerization of a biphotochromic molecule is a more disruptive to a bilayer membrane than **1** or **3**. Prior to UV irradiation, k_{K+} for **2** in DOPC vesicles at a mole ratio of 1:20 was two fold higher than the control vesicles, and 30% higher than **1** and **3** (Table 3). In DPPC vesicles, k_{K+} for **2** was similar to **1** and **3**. The % release for **2** was also two and three fold higher in DOPC and DPPC vesicles, respectively, than the control vesicles, and similar to both **1** and **3**. Again, this highlights the lower sensitivity of this assay to changes in molecular structure, as the large differences in k_{H+} between **2** and the monomers in DOPC vesicles were not apparent. Nonetheless, this assay is beneficial in examining the effect of photoisomerization on membrane permeability. Upon UV irradiation, the k_{K+} for **2** in DOPC vesicles increased 50%, whereas a two fold increase was observed in DPPC vesicles. By comparison, these rate constants were 50% higher than the monomers in DPPC vesicles, but similar in DOPC vesicles. In general, these increases also suggest that photoisomerization of spirooxazine dimer to its more polar ring-opened form leads to greater disruption of the local bilayer structure when compared with the nonirradiated vesicles. Like the monomer systems, upon visible irradiation a three fold decrease in k_{K+} was observed for **2** in DOPC vesicles, whereas a small reduction was found in DPPC vesicles. The net change in % release for **2** following irradiation was

three and 44 fold higher in DOPC and DPPC vesicles than the control vesicles, respectively. Interestingly, the molecular size of these spirooxazines is also positively correlated with net change in % release, particularly in DPPC vesicles. As a result, the photoinduced changes in ion permeation from lipid vesicles incorporating these (bola)amphiphilic spirooxazines is found to increase in the order of **3** < **1** < **2**. As shown earlier, the rate of thermal ring closure is highly dependent on the lipid bilayer phase state. Consequently, the variation in k_{K+} prior to, and upon UV and visible irradiation for these spirooxazines has a cumulative effect, which impacts the net change in % release. In DPPC vesicles, a trend with molecular size clearly emerges, whereas in DOPC vesicles this particular trend is less discernable. Overall, these results demonstrate that changes in membrane permeability can be reversibly photocontrolled with (bola)amphiphilic spirooxazines. We are currently examining the permeation of encapsulated molecules from lipid vesicles incorporating these spirooxazines. A preliminary study on the permeation of HPTS from DPPC vesicles incorporating **1** at a mole ratio of 1:40 shows that for each independent experiment a small net change in % release is observed upon UV irradiation when compared to nonirradiated vesicles (Figure 5). However, the average % release values are within experimental error of each other. As a result, further study is required to assess the activity of these spirooxazines as membrane disruptors for the delivery of small molecules from lipid vesicles. Moreover, we are currently exploring mixed lipid systems that produce coexisting liquid-disordered and liquid-ordered phase states.

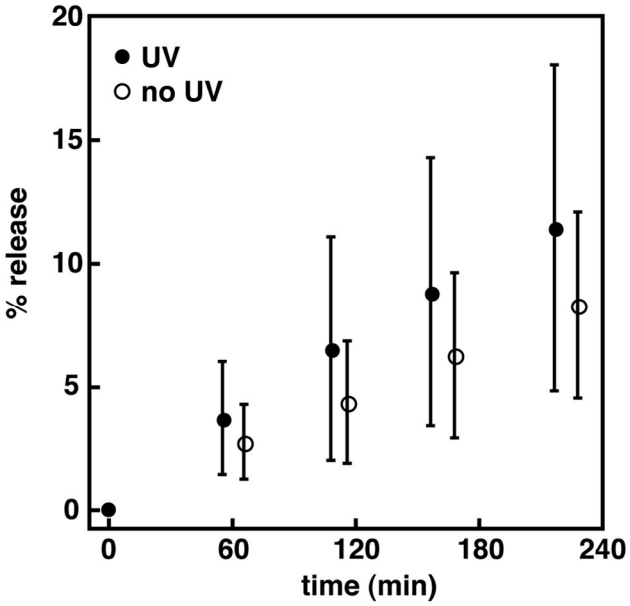

Figure 5. Normalized percentage of HPTS release as a function of time for **1** in DPPC vesicles at a mole ratio of 1:40 (i.e., spirooxazine/lipid) with and without periods of UV irradiation. The error is the standard deviation for the mean taken from five independent measurements.

Conclusions

In summary, we have synthesized (bola)amphiphilic spirooxazines and have examined their photochromism in organic solution and lipid vesicles. Solvent polarity and the lipid bilayer phase state have a large effect on the isomerization kinetics. Notably, the thermal ring closure rate constant for **2** was significantly lower in DPPC bilayers as the higher local viscosity of the gel phase and the large dimeric structure severely reduces the conformational flexibility required for spirooxazine isomerization. In addition, two ion permeation assays were used to assess the effect of spirooxazine inclusion and isomerization on the membrane permeability of lipid vesicles. In all cases, photoisomerization of the incorporated spirooxazines to their open-ring form disrupts the bilayer membrane structure and enhances permeability. However, ion permeation is clearly sensitive to the lipid bilayer phase state and the relative position of the photochromic moiety in the bilayer membrane. Overall, we have established that membrane permeability can be reversibly photocontrolled with (bola)amphiphilic spirooxazines.

Experimental

Supporting data tables and figures, and synthetic procedures, including NMR and high-resolution mass spectra, are described in the electronic supplementary information (ESI).

Instrumentation. ^{1}H and ^{13}C NMR spectra were recorded at 300.18 and 75.48 MHz, respectively, on a Varian Mercury plus spectrometer. Chemical shifts are referenced to solvent signals. ^{13}C NMR spectra were recorded with ^{1}H decoupling. High-resolution mass spectral analyses were carried out by the University of Calgary on a VG 70SE mass spectrometer and the University of Saskatchewan on a API Qstar XL mass spectrometer or JEOL AccuTOF-GCv 4G mass spectrometer, using various ionization techniques (e.g., chemical ionization, electron ionization, electrospray ionization, or field desorption). Steady-state absorption spectra and kinetics were obtained at constant temperature (e.g., 21.0 ± 0.1 °C) on a Cary 300 Bio UV–Vis spectrophotometer equipped with a dual cell Peltier circulator accessory. Absorption spectra were recorded at a scan rate, step size, and integration time of 300 nm min^{-1}, 0.5 nm, and 0.1 s, respectively. Kinetic measurements were recorded at the λ_{max} for the open-ring isomer following UV irradiation and with an integration time of 0.1 s. The effective rate constants for thermal equilibration (k_T) were determined from exponential fits of the absorbance decays at λ_{max}. In particular, $k_T = k_1 + k_{-1}$, where k_1 and k_{-1} are the thermal rate constants for the ring-opening and ring-closing reactions, respectively. Due to the detection limits of our instrumentation, we were unable to determine k_1 (i.e., $k_1 >> k_{-1}$). It has been shown previously for spirooxazines containing phenanthryl moieties that $k_{-1} \approx k_T$.[16] Thus to a good approximation, we will specifically refer to k_T as the rate constant for thermal ring closure. Steady-state fluorescence spectra were obtained at constant temperature (i.e., 21.0 ± 0.1 °C) with a PTI QuantaMaster spectrofluorometer, and the excitation and emission slits were set such that the bandwidths were 2 nm. Excitation ratio experiments using HPTS were

performed with excitation wavelengths of 403 and 460 nm and an emission wavelength of 510 nm. The integration time was 2 s. The emission experiments using HPTS were performed with an excitation wavelength of 413 and an emission wavelength range of 450-700 nm. The integration time was 0.25 s. Potassium ion permeation was monitored using a MI-442 K^+ ion microelectrode and a MI-402 Ag/AgCl reference microelectrode from Microelectrodes, which were connected to a Thermo Scientific Orion Star A325 meter. The electrode potentials were recorded once per minute. For the proton assay, all samples were irradiated with a 300 W xenon light source from Luzchem, and measured in a quartz Suprasil fluorescence cell (10 mm × 10 mm) from Hellma. For ultraviolet irradiations, the xenon light source was filtered with a bandpass filter (Hoya U-340, $\lambda_c = 340 \pm 42$ nm). For visible irradiations, a bandpass filter (Thorlabs FB530-10, $\lambda_c = 530 \pm 5$ nm) was used. For the potassium ion assay, all samples were measured in a quartz test tube (14 mm OD, 12 mm ID, 100 mm long) from Luzchem, which was positioned in a water-filled and water-jacketed beaker at constant temperature (i.e., 21.0 ± 0.1 °C). For ultraviolet irradiations, a 6 W UVA ($\lambda_c = 365$ nm) UltraLum TLC lamp was used. For visible irradiations, a 300 W Osram EXR halogen lamp of a Kodak Ektagraphic III E Plus slide projector fitted with a longpass filter (Schott GG-495, $\lambda_c = 495 \pm 6$ nm) was used. For the fluorescence assay, all samples were measured in a quartz fluorescence cell at constant temperature (i.e., 20.0 ± 0.1 °C), but irradiated in Pyrex test tubes. The tubes were loaded onto a rotating sample rack that was placed into a 2 L Pyrex beaker containing a cupric sulfate solution (100 mM) at constant temperature (20 ± 2 °C), which was positioned in a Rayonet RPR-100 photochemical reactor equipped with eight 8 W UVA ($\lambda_c = 350$ nm) lamps from Luzchem. For the kinetic studies, all samples were measured in a quartz fluorescence cell and irradiated with the 6 W UVA lamp for 20 s. The decay in absorbance was monitored at λ_{MC} until a constant baseline was obtained.

Materials. All reactants (99+%, Sigma-Aldrich), deuterated solvents (99.9 atom % D, Sigma-Aldrich), palladium catalysts (99.9+% Pd, Strem Chemicals), Triton X-100 (scintillation grade, Eastman Kodak Company), buffer salts (99+%, Sigma-Aldrich and Alfa Aesar), 1,2-dioleoyl-*sn*-glycero-3-phosphocholine (DOPC; >99%, Avanti Polar Lipids), and 1,2-dipalmitoyl-*sn*-glycero-3-phosphocholine (DPPC; >99%, Avanti Polar Lipids) were purchased and used as received. Copper (I) iodide, dimethyl formamide, 1,4-dioxane, tetrahydrofuran, and triethylamine were purified based on literature procedures.[46] Flash column chromatography was performed on silica gel (230-400 mesh, 60 Å, Sillicycle), neutral aluminum oxide (activated, 150 mesh, 58 Å, Sigma-Aldrich), and basic aluminum oxide (activated, 60 mesh, 58 Å, Alfa Aesar). 8-Hydroxypyrene-1,3,6-trisulfonic acid trisodium salt (HPTS; dye content ca. 75%, Sigma-Aldrich) was recrystallized from ethanol five times. Deionized water was obtained from a Milli-Q Gradient A10 water system (Millipore Corp.). All aqueous solutions were prepared in phosphate buffer (10 mM Na_3PO_4, 100 mM NaCl, pH adjusted to 6.4 using H_3PO_4). The organic solvents used in the absorption and kinetic studies were spectrophotometric grade.

Procedure for lipid vesicle preparation. The preparation of lipid vesicles has been previously described in detail.[47] The same procedures were used to prepare lipid vesicles for the proton and potassium ion permeability assays; however, higher lipid concentrations were used for the latter. The concentrations or volumes used for the proton and potassium ion assays are indicated in parentheses, respectively. Briefly, lipid stock solutions (2 or 10 mg/mL) of DOPC and DPPC were prepared in chloroform. Separate stock solutions of **1**–**3** in chloroform (1 mM), 8-hydroxypyrene-1,3,6-trisulfonic acid trisodium salt (HPTS; 10 μM) in phosphate buffer, and potassium chloride (0.20 M) in phosphate buffer were prepared. As an example, to prepare DDPC vesicles containing **2** at a mole ratio of 1:20 (**2**/DPPC), a stock solution of **2** (127 μL or 254 μL) and DPPC (1 mL or

400 μL) were added to a 10 mL round bottom flask. The chloroform was evaporated under reduced pressure to deposit a lipid film. The lipid film was dried under reduced pressure for at least 3 h and then hydrated with HPTS or potassium chloride (1 mL) at 50.0 ± 0.1 °C for a minimum of 3 h. The lipid suspension was left to stand overnight at 4 °C. The hydrated lipid suspension underwent five freeze and thaw cycles by placing the sample in a dry ice/acetone bath, followed by a warm water bath and vortexed for 30 s. The sample was extruded 21 times at constant temperature (50.0 ± 0.5 °C) using 0.1 μm polycarbonate membrane filters. The sample was loaded onto a buffered PD MidiTrap G-25 desalting column and eluted with 1.5 mL of buffer to remove extravesicular HPTS or potassium chloride. The first 5 drops of eluent were discarded to give a purified lipid vesicle sample (1.3 mg/mL or 2.7 mg/mL).

Proton permeability assay. The protocol for the HPTS fluorescence assay has been previously described.[14] Briefly, 2 mL of phosphate buffer and 100 μL of the lipid vesicle sample were transferred to a fluorescence cell and stirred. For nonirradiated samples, 50 μL of 0.5 M NaOH was added following a 150 s equilibration period. After 700 s, the vesicles were lysed with 50 μL of a 5% Triton X-100 solution. For irradiated samples, the base was added following a 70 s equilibration period, which was preceded by 3 min of UV irradiation, and an initial 80 s equilibration period. All data collected during the 150 s equilibration period and ca. 30 s after the addition of base was not used when fitting the data (i.e., ca. 180 s was t_0). The relative emission intensity E_{403}/E_{460} (I) was calculated and then the extent of ion permeation (N_t) was calculated using Eq. 1,

$$N_t = \frac{(I_t - I_0)}{(I_\infty - I_0)} \quad (1)$$

where I_t is the relative emission intensity at time t, I_0 is the relative emission intensity at t_0, and I_∞ is the relative emission intensity when the vesicles are lysed. The extent of ion permeation was plotted against time, and the slope from the linear fit represents the rate constant for proton permeation.

Potassium ion permeability assay. The protocol for the potassium ion assay has been adapted from a previously published procedure.[13] Briefly, 2 mL of phosphate buffer and 100 μL of the lipid vesicle sample were transferred to a quartz test tube and stirred. The microelectrodes were positioned into the quartz test tube and the potential of the diluted lipid vesicle sample was monitored continuously. Following an equilibration period, the sample was irradiated alternatively with UV (6 min) and visible (6 min) light for three and a half cycles. After irradiation, the vesicles were lysed with 50 μL of a 5% Triton X-100 solution. A calibration curve was prepared from the electrode potentials recorded at various concentrations of potassium chloride in phosphate buffer, ranging from 0.01 to 5.00 mM. A strong linear correlation was observed (i.e., $R^2 = 0.9968$, Figure S14). Using this calibration curve, potassium ion concentrations were determined and then plotted against time. The slope from the linear fit represents the rate constant for potassium ion permeation. The percent release was calculated using Eq. 2,

$$\%\ \text{release} = \frac{(c_t - c_0)}{(c_\infty - c_0)} \times 100\% \qquad (2)$$

where c_t is the potassium ion concentration at time t, c_0 is the potassium ion concentration at t_0, and c_∞ is the potassium ion concentration when the vesicles are lysed.

HPTS permeability assay. The protocol and the preparation of lipid vesicles for the HPTS self-quenching assay has been previously described in detail.[47] Briefly, 6 mL of phosphate buffer and

1.5 mL of the lipid vesicle sample were transferred to a Pyrex test tube. Following an equilibration period, the sample was irradiated consecutively with UV light for 60, 60, 180, and 600 s. After each irradiation, an aliquot of the sample (1.5 mL) was transferred to a quartz cell and the fluorescence spectrum was recorded. The final aliquot of lipid vesicles was lysed with Triton X-100 solution. The percent release was calculated from the baseline corrected fluorescence intensities at 510 nm using Eq. 3,

$$\%\ \text{release} = \frac{(I_t - I_0)}{(I_\infty - I_0)} \times 100\% \qquad (3)$$

where I_t is the emission intensity at time t, I_0 is the emission intensity at t_0, and I_∞ is the emission intensity when the vesicles are lysed.

Acknowledgments

We would like to express our gratitude to the Natural Sciences and Engineering Research Council (NSERC) of Canada, the Saskatchewan Health Research Foundation (SHRF), and the University of Regina for support of this work.

References

1. C. K. McKenzie, I. Sanchez-Romero and H. Janovjak, Flipping the Photoswitch: Ion Channels Under Light Control. In *Novel Chemical Tools to Study Ion Channel Biology*, 1st ed.; C. Ahern and S. Pless, Eds; Advances in Experimental Medicine and Biology Series; Springer-Verlag Berlin: Berlin, 2015, Vol. 869, pp 101–117.
2. R. Zappacosta, G. Siani, S. Silvi, A. Credi and A. Fontana, *Langmuir*, 2014, **30**, 13667–13672.

3. R. Tong, H. D. Hemmati, R. Langer and D. S. Kohane, *J. Am. Chem. Soc.*, 2012, **134**, 8848–8855.

4. N. Fomina, J. Sankaranarayanan and A. Almutairi, *Adv. Drug Deliv. Rev.*, 2012, **64**, 1005–1020.

5. A. Yavlovich, B. Smith, K. Gupta, R. Blumenthal and A. Puri, *Mol. Membr. Biol.*, 2010, **27**, 364–381.

6. J. Y. Wang, Q. F. Wu, J. P. Li, Q. S. Ren, Y. L. Wang and X. M. Liu, *Mini Rev. Med. Chem.*, 2010, **10**, 172–181.

7. F. Ercole, T. P. Davis and R. A. Evans, *Polym. Chem.*, 2010, **1**, 37–54.

8. C. Alvarez-Lorenzo, L. Bromberg and A. Concheiro, *Photochem. Photobiol.*, 2009, **85**, 848–860.

9. P. Shum, J.-M. Kim and D. H. Thompson, *Adv. Drug Delivery Rev.*, 2001, **53**, 273–284.

10. S. Matile, A. V. Jentzsch, J. Montenegro and A. Fin, *Chem. Soc. Rev.*, 2011, **40**, 2453–2474.

11. T. Sato, M. Kijima, Y. Shiga and Y. Yonezawa, *Langmuir*, 1991, **7**, 2330–2335.

12. Y. Lei and J. K. Hurst, *Langmuir*, 1999, **15**, 3424–3429.

13. R. F. Khairutdinov and J. K. Hurst, *Langmuir*, 2001, **17**, 6881–6886.

14. Y. S. Kandasamy, J. Cai, A. Beler, M.-S. J. Sang, P. D. Andrews and R. S. Murphy, *Org. Biomol. Chem.*, 2015, **13**, 2652–2663.

15. A. Zelichenok, F. Buchholtz, J. Ratner, E. Fischer and V. Krongauz, *J. Photochem. Photobiol., A*, 1994, **77**, 201–206.

16. R. F. Khairutdinov, K. Giertz, J. K. Hurst, E. N. Voloshina, N. A. Voloshin and V. I. Minkin, *J. Am. Chem. Soc.*, 1998, **120**, 12707–12713.

17. K. M. Louis, T. Kahan, D. Morley, N. Peti and R. S. Murphy, *J. Photochem. Photobiol., A*, 2007, **189**, 224–231.

18. S. Maeda, Spirooxazines. In *Organic Photochromic and Thermochromic Compounds*, J. C. Crano and R. J. Guglielmetti, Eds.; Plenum Press: New York, 1999; Vol. 1, pp 85–109.

19. V. I. Minkin, Photoswitchable Molecular Systems Based on Spiropyrans and Spirooxazines. In *Molecular Switches*, 2nd ed.; B. L. Feringa and W. R. Browne, Eds.; Wiley-VCH: Weinheim, 2011; Vol. 2, pp 37–80.

20. T. Stafforst and D. Hilvert, *Chem. Commun.*, 2009, 287–288.

21. D. Movia, A. Prina-Mello, Y. Volkov and S. Giordani, *Chem. Res. Toxicol.*, 2010, **23**, 1459–1466.

22. M. Hammarson, J. R. Nilsson, S. M. Li, T. Beke-Somfai and J. Andreasson, *J. Phys. Chem. B*, 2013, **117**, 13561–13571.

23. D. L. Watkins and T. Fujiwara, *J. Photochem. Photobiol., A*, 2012, **228**, 51–59.

24. W. Zhou, H. Zhang, H. Li, Y. Zhang, Q.-C. Wang and D.-H. Qu, *Tetrahedron*, 2013, **69**, 5319–5325.

25. D. L. Watkins and T. Fujiwara, *J. Mater. Chem. C*, 2013, **1**, 506–514.

26. A. Fihey, A. Perrier, W. R. Browne and D. Jacquemin, *Chem. Soc. Rev.*, 2015, **44**, 3719–3759.

27. H. Doucet, *Eur. J. Org. Chem.*, 2008, 2013–2030.

28. A. K. L. Yuen and C. A. Hutton, *Tetrahedron Lett.*, 2005, **46**, 7899–7903.

29. G. Favaro, F. Masetti, U. Mazzucato, G. Ottavi, P. Allegrini and V. Malatesta, *J. Chem. Soc., Faraday Trans.*, 1994, **90**, 333–338.

30. A. K. Chibisov and H. Görner, *J. Phys. Chem. A*, 1999, **103**, 5211–5216.

31. Y. R. Yi and I. J. Lee, *J. Photochem. Photobiol., A*, 2002, **151**, 89–94.

32. V. I. Minkin, *Chem. Rev.*, 2004, **104**, 2751–2776.

33. G. Favaro, F. Ortica and V. Malatesta, *J. Chem. Soc., Faraday Trans.*, 1995, **91**, 4099–4103.

34. S. Kumar, D. L. Watkins and T. Fujiwara, *Chem. Commun.*, 2009, 4369–4371.

35. D. Marsh, *Handbook of Lipid Bilayers*, 2nd ed.; CRC Press: Boca Raton, 2013.

36. C. J. Wohl, M. A. Helms, J. O. Chung and D. Kuciauskas, *J. Phys. Chem. B*, 2006, **110**, 22796–22803.

37. H. A. Stern and S. E. Feller, *J. Chem. Phys.*, 2003, **118**, 3401–3412.

38. T. M. Fyles and H. Luong, *Org. Biomol. Chem.*, 2009, **7**, 733–738.

39. S. Matile and N. Sakai, The Characterization of Synthetic Ion Channels and Pores. In *Analytical Methods in Supramolecular Chemistry*, C. A. Schalley, Ed.; Wiley-VCH: Weinheim, 2007, pp 391–418.

40. C. L. Kuyper, J. S. Kuo, S. A. Mutch and D. T. Chiu, *J. Am. Chem. Soc.*, 2006, **128**, 3233–3240.

41. S. Paula and D. W. Deamer, Membrane Permeability Barriers to Ionic and Polar Solutes. In *Membrane Permeability*, D. W. Dreamer, A. Kleinzeller and D. M. Fambrough, Eds.; Academic Press: San Diego, 1999, pp 77–95.

42. K. A. Runas and N. Malmstadt, *Soft Matter*, 2015, **11**, 499–505.

43. O. Mertins, I. O. L. Bacellar, F. Thalmann, C. M. Marques, M. S. Baptista and R. Itri, *Biophys. J.*, 2014, **106**, 162–171.

44. W. Caetano, P. S. Haddad, R. Itri, D. Severino, V. C. Vieira, M. S. Baptista, A. P. Schröder and C. M. Marques, *Langmuir*, 2007, **23**, 1307–1314.

45. N. A. Porter, S. E. Caldwell and K. A. Mills, *Lipids*, 1995, **30**, 277–290.

46. D. D. Perrin and W. L. Armarego, *Purification of Laboratory Chemicals*; 3rd ed.; Elsevier Science: New York, 1988.

47. Y. Bai, K. M. Louis and R. S. Murphy, *J. Photochem. Photobiol., A*, 2007, **192**, 130–141.